Numerical studies on ultrarelativistic ion motions in an oblique magnetosonic shock wave

doi: 10.1063/1.3270110

Numerical studies on ultrarelativistic ion motions in an oblique magnetosonic shock wave

Shunsuke Usami, Ritoku Horiuchi, and Yukiharu Ohsawa

Citation: Phys. Plasmas **16**, 122104 (2009); doi: 10.1063/1.3270110
View online: http://dx.doi.org/10.1063/1.3270110
View Table of Contents: http://pop.aip.org/resource/1/PHPAEN/v16/i12
Published by the American Institute of Physics.

Numerical studies on ultrarelativistic ion motions in an oblique magnetosonic shock wave

Shunsuke Usami,[1,a)] Ritoku Horiuchi,[1,2] and Yukiharu Ohsawa[3]
[1]*Department of Simulation Science, National Institute for Fusion Science, Toki 509-5292, Japan*
[2]*The Graduate University for Advanced Studies, Toki 509-5292, Japan*
[3]*Department of Physics, Nagoya University, Nagoya 464-8602, Japan*

(Received 2 June 2009; accepted 6 November 2009; published online 4 December 2009)

The motion of ultrarelativistic ions in an oblique magnetosonic shock wave is studied analytically and numerically. The zeroth-order theory predicts that an oblique shock wave can accelerate ions in the direction nearly parallel to the magnetic field if the shock speed is $v_{sh} \sim c \cos\theta$, where θ is the angle between the wave normal and the magnetic field, while the perturbation is a one-dimensional oscillation nearly perpendicular to the zeroth-order motion. The perturbation frequency ω is of the order of $\Omega_{i0}\gamma^{-1/2}$, where γ is the Lorentz factor of the zeroth-order velocity. These theoretical predictions are examined with test particle simulations, in which the test particle orbits are calculated with use of the electromagnetic fields of a shock wave obtained from an electromagnetic particle simulation. The zeroth-order and perturbed motions in the simulations are explained by the theory. © *2009 American Institute of Physics*. [doi:10.1063/1.3270110]

I. INTRODUCTION

Several nonstochastic particle acceleration mechanisms occurring in magnetosonic shock waves have been studied with theory and particle simulations;[1–20] for instance, the sharp rise of the electric potential and the magnetic field in the shock transition region energize some ions by reflecting them,[1–9] and acceleration to relativistic energies has been demonstrated with particle simulations.[4] In a multi-ion-species plasma in which protons are the major ion component as in space plasmas, all the heavy ions gain energy from the transverse electric field when they pass through the shock transition region and have nearly the same speed;[10] these results have been applied to solar energetic particles to explain the observations that the elemental compositions of solar energetic heavy ions are similar to that of the solar corona.[21] Some electrons can be trapped by a shock wave and are accelerated to ultrarelativistic energies with the Lorentz factors $\gamma > 100$.[11] Relativistic ions can stay near the shock transition region for periods much longer than their relativistic gyroperiods, during which their energies go up stepwise.[17] Particle simulations have thus demonstrated particle acceleration to energies much higher than those of solar energetic particles (the highest energies of solar energetic electrons and ions are, respectively, several tens of megaelectronvolts ($\gamma \sim 100$) and 1–10 GeV ($\gamma = 1 \sim 10$).

In a mechanism recently found,[18,20] a shock wave accelerates particles along the magnetic field with its electric field parallel to the magnetic field, $E_\parallel = (\boldsymbol{E}\cdot\boldsymbol{B})/B$. Since the integral of the parallel electric field along the magnetic field, $F = -\int E_\parallel ds$, rises in the shock transition region[22] as the electric potential does, positively charged particles, such as ions and positrons, can suffer this acceleration (positrons could be present around pulsars[23,24]). The accelerated particles stay in the shock transition region for long periods of time, move nearly parallel to the magnetic field $\boldsymbol{B}$, and absorb energy from $E_\parallel$.

If the Lorentz factor γ of a particle is much greater than unity, then even a slight increase in the particle speed v would result in a huge increase in γ. By use of this fact, an acceleration theory has been developed,[18] in which the zeroth-order velocity $\boldsymbol{v}_0$ is parallel to the external magnetic field $\boldsymbol{B}_0$. The zeroth-order theory is applicable to both the ions and positrons, while for the perturbations around the zeroth-order motion, two different theoretical schemes have been presented; one for positrons and the other for ions.[20]

The theory for the positrons predicts that their perturbed motion is elliptic in the plane nearly perpendicular to $\boldsymbol{v}_0$ and the frequency of the perturbed motion is of the order of the relativistic gyrofrequency.[20] These predictions have been verified with relativistic particle simulations. That is, the simulations have demonstrated that an oblique magnetosonic shock wave in an electron-positron-ion plasma accelerates some positrons in the direction parallel to the magnetic field to energies $\gamma \sim 2000$ (Fig. 1 in Ref. 19); the acceleration processes continued till the end of the simulation run ($\omega_{pe}t = 5000$), suggesting that the particle energies would further rise if we carry out longer time simulations. Furthermore, the observed perturbation motions and frequencies were consistent with the theoretical predictions.

The theory for the ions,[20] however, has not been tested yet with computer experiments. In this paper, we investigate the motions of ultrarelativistic ions with numerical simulations and compare them with the theory. In Sec. II, we briefly describe the theory of the motion of an ion accelerated parallel to the magnetic field. The ion perturbation motion is one-dimensional with frequency of the order of $\Omega_{i0}\gamma^{-1/2}$, where Ω_{i0} is the nonrelativistic ion gyrofrequency, and its velocity $\boldsymbol{v}_1$ is nearly perpendicular to the zeroth-order velocity $\boldsymbol{v}_0$. In Sec. III, we perform test particle simulations. First, we carry out a simulation of a shock wave using a one-

a)Electronic mail: usami.shunsuke@nifs.ac.jp.

dimensional (one space coordinate and three velocities), fully kinetic, relativistic, electromagnetic particle code and obtain the electric and magnetic fields of the shock wave. Assuming that the wave propagation is stationary, we then follow the trajectories of energetic test ions in these fields. This method enables us to follow ion orbits for long periods of time, much longer than the ion gyroperiod, and to precisely test the theory described in Sec. II, removing the effect of the change in the wave profile. The simulations demonstrate that some ions are accelerated along the magnetic field in a shock wave. The case with unstable perturbations is also shown. In both the stable and unstable cases, the observed zeroth-order and perturbation motions are consistent with the theory. Section IV gives a summary of our work.

II. OVERVIEW OF THE THEORY

We outline the theory of acceleration of ultrarelativistic ions along the magnetic field.[20] By using the relativistic equation of motion

$$m_i \frac{d(\gamma \boldsymbol{v})}{dt} = q_i \left(\boldsymbol{E} + \frac{\boldsymbol{v}}{c} \times \boldsymbol{B} \right), \tag{1}$$

we analyze ion motions in a stationary, one-dimensional $(\partial/\partial y = \partial/\partial z = 0)$ plasma wave propagating in the x direction with a speed v_{sh} in an external magnetic field $\boldsymbol{B}_0 = (B_{x0}, 0, B_{z0}) = B_0(\cos\theta, 0, \sin\theta)$. In Secs. II A and II B, no specific wave mode is assumed. In Sec. II C, we consider magnetosonic shock waves and estimate the time rate of change of γ of an ion accelerated with this mechanism.

A. Zeroth-order motion

If the Lorentz factor γ is much greater than unity, a slight change in the particle speed leads to a great change in γ. Therefore, assuming that

$$|\boldsymbol{v}| \frac{d\gamma}{dt} \gg \gamma \left| \frac{d\boldsymbol{v}}{dt} \right|, \tag{2}$$

we ignore the term $\gamma d\boldsymbol{v}/dt$ in Eq. (1), which yields the equation for the zeroth-order velocity $\boldsymbol{v}_0$

$$m_i \frac{d\gamma_0}{dt} \boldsymbol{v}_0 = q_i \left(\boldsymbol{E} + \frac{\boldsymbol{v}_0}{c} \times \boldsymbol{B} \right), \tag{3}$$

where γ_0 is the zeroth-order Lorentz factor.

If the x component of $\boldsymbol{v}_0$ is given by

$$v_{x0} = v_{\mathrm{sh}}, \tag{4}$$

then this particle can move with the wave for a long time. By virtue of Eq. (4) and the relations $E_y = (v_{\mathrm{sh}}/c)(B_z - B_{z0})$ and $E_z = -(v_{\mathrm{sh}}/c)B_y$, which hold for stationary waves, Eq. (3) becomes

$$m_i v_{\mathrm{sh}} \frac{d\gamma_0}{dt} = q_i \left(E_x + \frac{v_{y0}}{c} B_z - \frac{v_{z0}}{c} B_y \right), \tag{5}$$

$$m_i v_{y0} \frac{d\gamma_0}{dt} = q_i \left(\frac{v_{z0}}{c} B_{x0} - \frac{v_{\mathrm{sh}}}{c} B_{z0} \right), \tag{6}$$

$$m_i v_{z0} \frac{d\gamma_0}{dt} = -q_i \frac{v_{y0}}{c} B_{x0}. \tag{7}$$

For $\gamma \gg 1$, we find that

$$v_{y0} = -\frac{E_x B_{z0} v_{\mathrm{sh}} \gamma_{\mathrm{sh}}^{-2} - B_{x0} B_y c \gamma_{\mathrm{sh}}^{-4}}{B_{z0} B_z (v_{\mathrm{sh}}/c) \gamma_{\mathrm{sh}}^{-2} + B_{z0}^2 (v_{\mathrm{sh}}/c)^3}, \tag{8}$$

$$v_{z0} = \frac{B_{x0}}{B_{z0}} \frac{c^2 \gamma_{\mathrm{sh}}^{-2}}{v_{\mathrm{sh}}}, \tag{9}$$

$$\frac{d\gamma_0}{dt} = \left(\frac{q_i}{m_i c} \right) \frac{E_x B_{z0} (v_{\mathrm{sh}}/c) - B_{x0} B_y \gamma_{\mathrm{sh}}^{-2}}{B_z \gamma_{\mathrm{sh}}^{-2} + B_{z0} (v_{\mathrm{sh}}/c)^2}, \tag{10}$$

where $\gamma_{\mathrm{sh}} = [1 - (v_{\mathrm{sh}}/c)^2]^{-1/2}$.

If the wave speed is close to $c \cos\theta$,

$$v_{\mathrm{sh}} \simeq c \cos\theta, \tag{11}$$

then the particles with $v_{\parallel} \simeq c$, where $v_{\parallel}$ is the speed along the magnetic field, would be able to interact with the wave for long periods of time. For the wave speed (11), γ_{sh} is approximated as $\gamma_{\mathrm{sh}}^{-1} \simeq \sin\theta$. Then, $\boldsymbol{v}_0$ and $d\gamma_0/dt$ may be written as

$$v_{y0} = -\left(\frac{E_x - (v_{\mathrm{sh}}/c) B_y \tan\theta}{B_{x0} \cot\theta + B_z} \right) c, \tag{12}$$

$$\frac{v_{z0}}{v_{\mathrm{sh}}} = \frac{B_{z0}}{B_{x0}}, \tag{13}$$

$$\frac{d\gamma_0}{dt} = \frac{q_i B_{x0}}{m_i v_{\mathrm{sh}}} \left(\frac{E_x - (v_{\mathrm{sh}}/c) B_y \tan\theta}{B_z \tan\theta + B_{x0}} \right) = \Omega_{i0} \frac{c \cos\theta}{v_{\mathrm{sh}}} \frac{(\boldsymbol{E} \cdot \boldsymbol{B})}{(\boldsymbol{B} \cdot \boldsymbol{B}_0)}, \tag{14}$$

where $\Omega_{i0} = q_i B_0/(m_i c)$. In the second equation of Eq. (14), we have used the relations $E_z = -(v_{\mathrm{sh}}/c) B_y$ and $\boldsymbol{E} \cdot \boldsymbol{B} = \boldsymbol{E} \cdot \boldsymbol{B}_0$, which are obtained from Faraday's law for stationary, one-dimensional waves.

For the wave speed (11), $|v_{y0}|$ is much smaller than v_{x0} and v_{z0}; Eq. (13) then indicates that $\boldsymbol{v}_0$ is nearly parallel to $\boldsymbol{B}_0$.

B. First-order motion

We now describe the perturbations around the zeroth-order solution. We expand the particle position and velocity as

$$\boldsymbol{x} = \boldsymbol{x}(0) + \boldsymbol{v}_0 t + \epsilon \boldsymbol{x}_1(t) + \epsilon^2 \boldsymbol{x}_2(t) + \cdots, \tag{15}$$

$$\boldsymbol{v} = \boldsymbol{v}_0 + \epsilon' \boldsymbol{v}_1(t) + (\epsilon')^2 \boldsymbol{v}_2(t) + \cdots, \tag{16}$$

where $\boldsymbol{x}(0)$ is the initial position, and ϵ and ϵ' are smallness parameters. [In writing the expansion in the form of (15) and (16), we view the quantities $\boldsymbol{x}_1$ and $\boldsymbol{v}_1$ are of the same order of magnitudes.] The relation $d\gamma/dt = [\gamma^3/(2c^2)] dv^2/dt$ indicates that a small change in v creates a large change in γ. Then, introducing a parameter Γ of the order of γ,

$$\Gamma \sim \gamma \gg 1, \tag{17}$$

we assume the following ordering:

$$\frac{1}{\Omega_{i0}}\frac{d}{dt}\frac{v_0}{c} \sim \frac{1}{\Gamma^3}, \frac{1}{\Omega_{i0}}\frac{d\boldsymbol{v}_1}{dt} \sim \frac{\boldsymbol{v}_1}{\Gamma^{1/2}}, \quad \boldsymbol{v}_0 \cdot \boldsymbol{v}_1 \sim \frac{v_0 v_1}{\Gamma^2}. \tag{18}$$

(For the case of positrons, $d\boldsymbol{v}_1/dt$ was taken to be $\sim \boldsymbol{v}_1/\Gamma$.[20]) From Eqs. (15) and (16) and the second ordering in Eq. (18), we see that

$$\boldsymbol{\epsilon}' \sim \Gamma^{-1/2}\boldsymbol{\epsilon}. \tag{19}$$

We introduce the quantity

$$\xi = x - v_{\rm sh}t. \tag{20}$$

Because the wave is stationary, its fields depend only on ξ. The particle is supposed to move around its zeroth-order trajectory ξ_0 [$=x(0)$]. We expand the field quantities near this point as

$$E_x(\xi) = E_x(\xi_0) + \frac{dE_x}{d\xi_0}(\xi - \xi_0) + \cdots, \tag{21}$$

where $dE_x/d\xi_0$ represents the value of $dE_x(\xi)/d\xi$ at $\xi=\xi_0$.

Then, in the order of $\boldsymbol{\epsilon}$, the equation of motion becomes

$$\frac{v_{\rm sh}\gamma_0^3}{c^2}\left(\boldsymbol{v}_0 \cdot \frac{d\boldsymbol{v}_1}{dt}\right) + \gamma_0\frac{dv_{x1}}{dt} = f_x' x_1, \tag{22}$$

$$\frac{v_{y0}\gamma_0^3}{c^2}\left(\boldsymbol{v}_0 \cdot \frac{d\boldsymbol{v}_1}{dt}\right) + \gamma_0\frac{dv_{y1}}{dt} = 0, \tag{23}$$

$$\frac{v_{z0}\gamma_0^3}{c^2}\left(\boldsymbol{v}_0 \cdot \frac{d\boldsymbol{v}_1}{dt}\right) + \gamma_0\frac{dv_{z1}}{dt} = 0, \tag{24}$$

where f_x' is defined as

$$f_x' = \frac{q_i}{m_i}\left(\frac{dE_x}{d\xi_0} + \frac{v_{y0}}{c}\frac{dB_z}{d\xi_0} - \frac{v_{z0}}{c}\frac{dB_y}{d\xi_0}\right). \tag{25}$$

Now, assuming that the perturbed quantities vary with time as $\exp(-i\omega t)$, we find from Eqs. (22)–(24) the frequency ω as

$$\omega^2 = -\frac{f_x'}{\gamma_0\gamma_{\rm sh}^2}, \tag{26}$$

which indicates that ω^2 becomes positive if

$$f_x' < 0. \tag{27}$$

In this case, the perturbation is stable. The perturbation velocity $\boldsymbol{v}_1$ is one-dimensional with

$$\boldsymbol{v}_1 \propto \left(1, -\gamma_{\rm sh}^2\frac{v_{\rm sh}v_{y0}}{c^2}, -\gamma_{\rm sh}^2\frac{v_{\rm sh}v_{z0}}{c^2}\right), \tag{28}$$

which yields

$$\boldsymbol{v}_0 \cdot \boldsymbol{v}_1 = \frac{v_{x1}v_{\rm sh}\gamma_{\rm sh}^2}{\gamma_0^2}. \tag{29}$$

This is consistent with the third relation in the ordering (18).

C. Estimate of energy increase rate for a shock wave

To this point, we have made no assumption on the wave mode. We now consider magnetosonic shock waves and make an estimate of the time rate of change of γ, Eq. (14). Recent studies of nonlinear magnetosonic waves[22] have revealed that the magnitude of the parallel pseudopotential F, which is the integral of the parallel electric field along the magnetic field

$$F = -\int E_\parallel ds = -\int E_\parallel \frac{B}{B_{x0}}dx, \tag{30}$$

is given as

$$eF \sim (m_i v_{\rm A}^2 + \Gamma_e T_e)\frac{B_{z1}}{B_0}, \tag{31}$$

in shock waves, where $v_{\rm A}$ is the Alfvén speed, Γ_e is the specific heat ratio of electrons, T_e is the electron temperature, and B_{z1} is the perturbed magnetic field in the z direction. (This is the expression for large-amplitude waves. For small-amplitude magnetosonic waves, we have a slightly different form for F.[22]) From Eqs. (30) and (31), we can make an order estimation of the parallel electric field $E_\parallel$ as

$$E_\parallel \sim \frac{B_{x0}}{B}\frac{F}{\Delta}, \tag{32}$$

where Δ is the width of a shock transition region ($\sim c/\omega_{\rm pi}$). Substituting Eq. (32) in Eq. (14) yields

$$\frac{d\gamma_0}{dt} \sim \frac{B_{x0}^2(m_i v_{\rm A}^2 + \Gamma_e T_e)}{m_i v_{\rm sh}(c/\omega_{pi})(\boldsymbol{B}\cdot\boldsymbol{B}_0)}\frac{B_{z1}}{B_0}. \tag{33}$$

III. SIMULATION

We further investigate the acceleration mechanism discussed in Sec. II with computer simulations. In this method, we first obtain the electromagnetic fields in a shock wave from a one-dimensional, fully kinetic, electromagnetic, particle simulation and then carry out test particle calculations, in which we follow test particle orbits in these fields with use of Adams–Bashforth–Moulton method,[25,26] assuming that the shock propagation is stationary. [A shock wave can have various types of fluctuations, including microscopic thermal fluctuations. Macroscopic wave profile would vary with a time scale $(c/\omega_{\rm pi})/v_{\rm A}$, which is of the order of the ion gyroperiod. Some kinetic effects also give rise to the variation of the wave form: For instance, ion reflection from the shock front can create an amplitude-oscillation near the shock front,[27] the period of which is also $\sim\Omega_i^{-1}$. The time scale of the ion acceleration investigated in this paper is much longer than the ion gyroperiod.]

A. Particle simulation

The parameters of the particle simulation are as follows. The total system length is $L_x=8192\Delta_g$, where Δ_g is the grid spacing. The total number of electrons is $N_e=576\,000$; as in space plasmas, the code contains hydrogen and helium ions with the number of the latter being 10% of that of the former ($n_{\rm He}/n_{\rm H}=1/10$). The hydrogen-to-electron mass ratio was

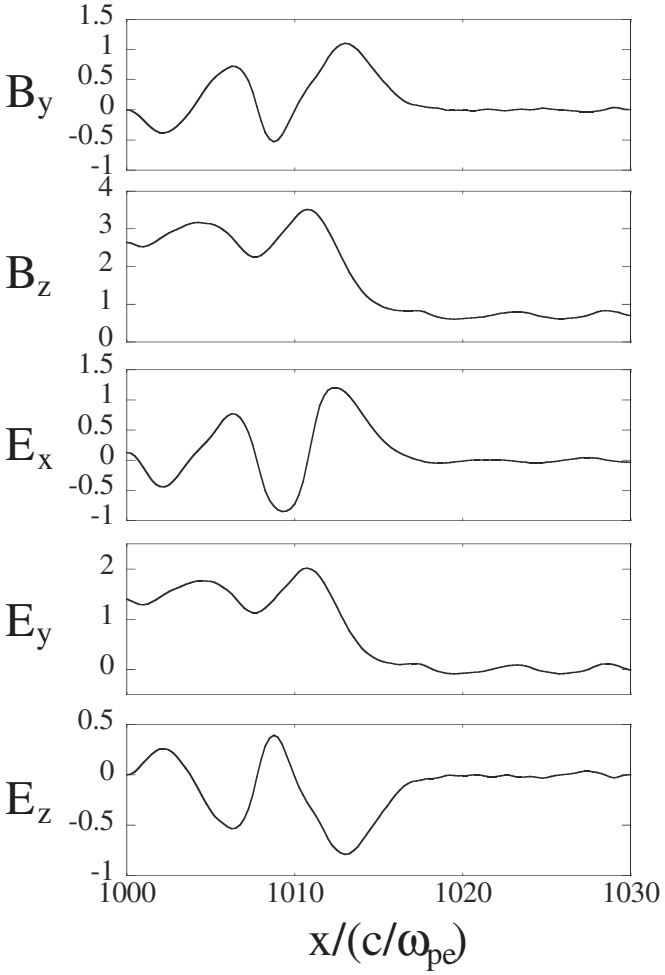

FIG. 1. Snapshot of field profiles in an oblique magnetosonic shock wave observed at $\omega_{pe}t=1200$ in a particle simulation. The fields are normalized to B_0. The shock speed is $v_{sh}=1.79v_A$, and the propagation angle is $\theta=45°$. The fields B_z and E_y have similar profiles, while B_y, E_x, and E_z are approximately proportional to $\partial B_z/\partial x$.

$m_H/m_e=50$. The ratio of the electron gyrofrequency to plasma frequency is $|\Omega_{e0}|/\omega_{pe}=3.0$ in the upstream region. The Alfvén speed $B_0/[4\pi(n_H m_H+n_{He}m_{He})]^{1/2}$ is therefore $v_A/c=0.39$. The electron skin depth is $c/(\omega_{pe}\Delta_g)=4$. The external magnetic field $\boldsymbol{B}_0$ is in the (x,z) plane, and the waves propagate in the x direction. The propagation angle θ is taken to be $\theta=45°$. The time step is $\omega_{pe}\Delta t=0.05$.

Figure 1 shows the electromagnetic-field profiles of a shock wave obtained from this particle simulation. Because B_x is constant, it is not shown here. The shock speed is observed to be $v_{sh}=1.79v_A$; thus, the relation (11) is satisfied.

In Fig. 2, we plot the profile of f_x' for the electromagnetic fields shown in Fig. 1. There exist regions where f_x' is negative; for which Eq. (27) predicts perturbed ion motions are stable.

B. Test particle simulation

We show two (stable and unstable) cases of test particle calculations. First, the stable case is discussed: We describe the motion of a relativistic hydrogen ion that is initially put at the location $x/(c/\omega_{pe})=1013.3$. At this point, $f_x'<0$, and

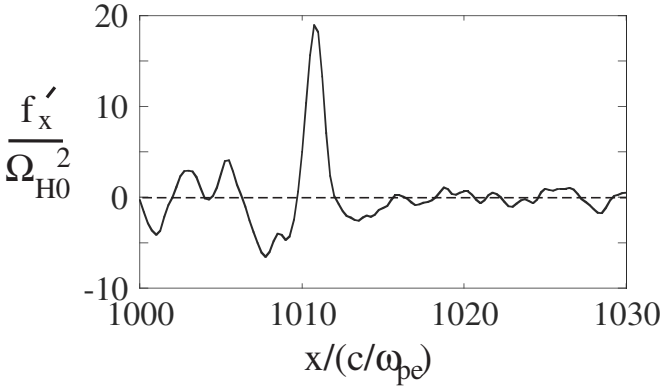

FIG. 2. Profile of f_x' calculated from the electromagnetic fields in Fig. 1. Here, Ω_{H0} is the nonrelativistic gyrofrequency of hydrogen ions.

thus the stability condition (27) is satisfied. According to Eqs. (4), (12), and (13), we decide the zeroth-order velocity of the test particle as $\boldsymbol{v}_0/c\simeq(0.700,-0.119,0.704)$. Figure 3 displays the time variations of the velocity components of the relativistic ion with initial energy $\gamma_0=100$. With these initial position and velocity, this particle is accelerated along the magnetic field as predicted in Sec. II. Its velocity $\boldsymbol{v}$ is almost constant until $\Omega_{H0}t\simeq1250$, at which the particle is detrapped and the acceleration ceases. [Although Fig. 1 showed the snapshots at $\omega_{pe}t=1200$ ($\Omega_{H0}t=72$), the time is normalized to the nonrelativistic ion gyroperiod Ω_{H0}^{-1} in Figs. 3 and 4, which is because the time scale is much longer in Figs. 3 and 4 than in Fig. 1.]

The upper panel of Fig. 4 shows the time variation of the Lorentz factor γ of this relativistic ion. This particle is ac-

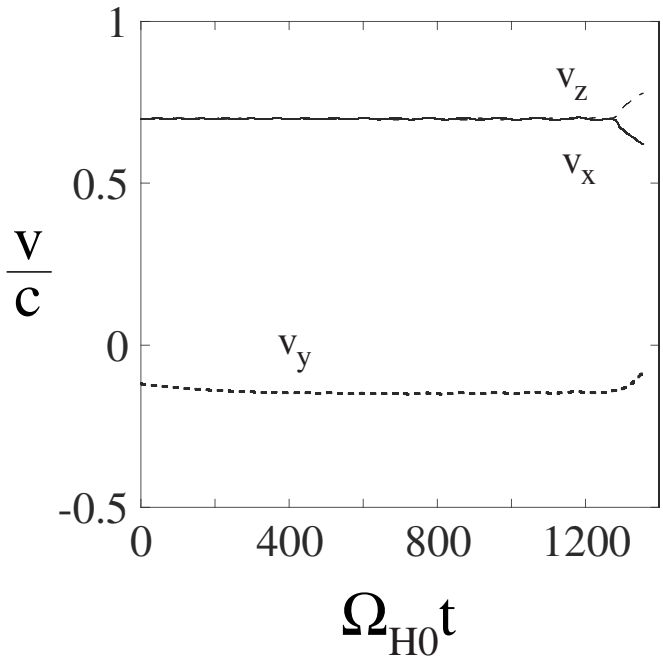

FIG. 3. Time variations of the velocities v_x, v_y, and v_z of an accelerated relativistic ion. The initial conditions for the position and velocity for the acceleration are satisfied (the initial energy is $\gamma_0=100$). The velocity $\boldsymbol{v}$ is almost constant until $\Omega_{H0}t\simeq1250$. Since $\theta=45°$, $v_x\simeq v_z$ during the acceleration phase.

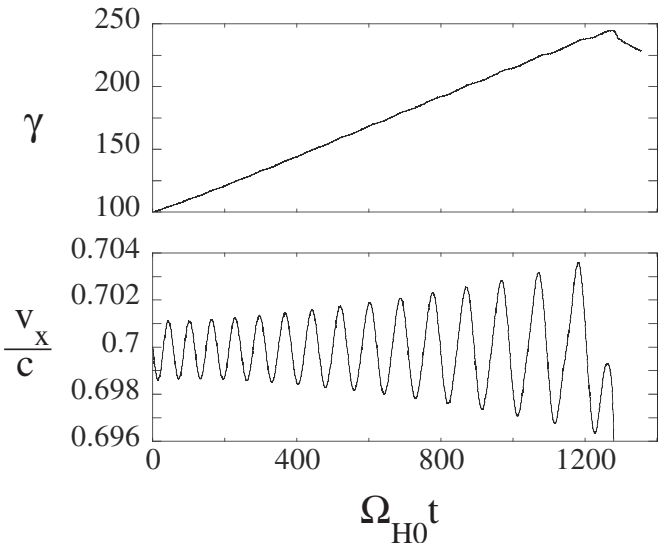

FIG. 4. Time variations of γ and v_x of an accelerated ion. The Lorentz factor γ increases almost linearly in time until $\Omega_{H0}t \simeq 1250$, and v_x exhibits small-amplitude oscillation.

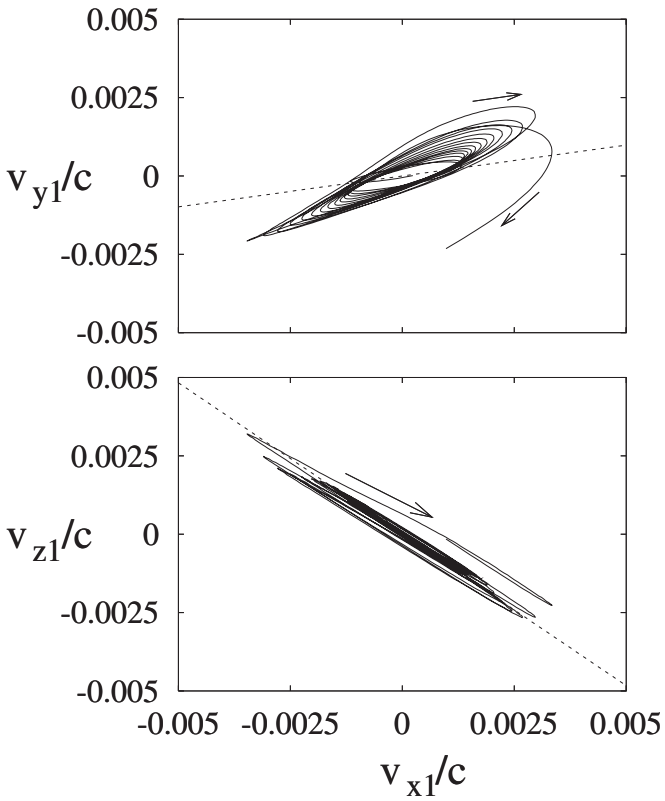

FIG. 5. Trajectories of ion perturbed velocities in the (v_{x1}, v_{y1}) and (v_{x1}, v_{z1}) planes. The dashed lines show the theoretical relations $v_{y1} = -(\gamma_{sh}^2 v_{sh} v_{y0}/c^2) v_{x1}$ (upper panel) and $v_{z1} = -(\gamma_{sh}^2 v_{sh} v_{z0}/c^2) v_{x1}$ (lower panel).

celerated for the period $0 \leq \Omega_{H0}t \leq 1250$, during which its energy increases almost linearly in time from $\gamma = 100$ to $\gamma \simeq 250$. The time rate of change of γ is observed to be $d\gamma/d(\Omega_{H0}t) \simeq 0.117$. This is close to the theoretical value $d\gamma/d(\Omega_{H0}t) = 0.120$, which we have obtained by substituting the initial values v_{y0} and v_{z0} in Eq. (7). [We can also adopt Eq. (14) to obtain this quantity. If we use observed values of $\langle (\boldsymbol{E}\cdot\boldsymbol{B})/(\boldsymbol{B}\cdot\boldsymbol{B}_0)\rangle$ in Eq. (14), where the brackets indicate the average over the time from $\Omega_{H0}t = 0$ to $\Omega_{H0}t = 1250$, we obtain $d\gamma/d(\Omega_{H0}t) = 0.102$, which is consistent with the above two values. Furthermore, Eq. (33), which was obtained with use of the order estimate of the parallel electric field, also gives the same order of magnitude $d\gamma/d(\Omega_{H0}t) \simeq 0.162$.]

In the lower panel of Fig. 4, the time variation of v_x is depicted. It oscillates around the zeroth-order value $v_{x0} = v_{sh}$. The oscillation period becomes longer as the energy rises, which is quantitatively examined below in Fig. 7.

Figure 5 displays the orbits of this ion in the (v_{x1}, v_{y1}) and (v_{x1}, v_{z1}) planes, where $\boldsymbol{v}_1 = \boldsymbol{v} - \boldsymbol{v}_0$. The dashed lines represent the relations between the perturbed velocities, $v_{y1} \simeq 0.163 v_{x1}$ (upper panel) and $v_{z1} \simeq 0.966 v_{x1}$ (lower panel), given by the theory Eq. (28). Since $\boldsymbol{v}_0$ slightly varies with time, and $\boldsymbol{v}_1$ oscillates, we have used $\boldsymbol{v}_0(t)$ averaged over each oscillation period in calculating $\boldsymbol{v}_1 = \boldsymbol{v} - \boldsymbol{v}_0$. The trajectories are near the theoretical dashed lines. We note also, however, that in the late phase of the oscillation, the value of v_{y1} moves away from the dashed line, which may be the sign of the breakdown of the acceleration.

We show in Fig. 6 the time variation of the parallel component of $\boldsymbol{v}_1$ to $\boldsymbol{v}_0$, $|(\boldsymbol{v}_0/v_0)\cdot\boldsymbol{v}_1|/\langle v_1\rangle$. The values of $|(\boldsymbol{v}_0/v_0)\cdot\boldsymbol{v}_1|/\langle v_1\rangle$ are much smaller than unity until $\Omega_{H0}t \simeq 1100$, which verifies that $\boldsymbol{v}_1$ is nearly perpendicular to $\boldsymbol{v}_0$.

We plot in Fig. 7 the perturbation frequency ω as a function of γ_0. The perturbation frequency varies in proportion to $\gamma_0^{-1/2}$. The simulation results (dots) fit well to the theoretical curve given by Eq. (26); in the estimate of Eq. (26), we have used the simulation values of f_x'.

Figure 8 shows an unstable case. Here, the initial particle position is $x/(c/\omega_{pe}) = 1011.2$, at which f_x' is positive. If the

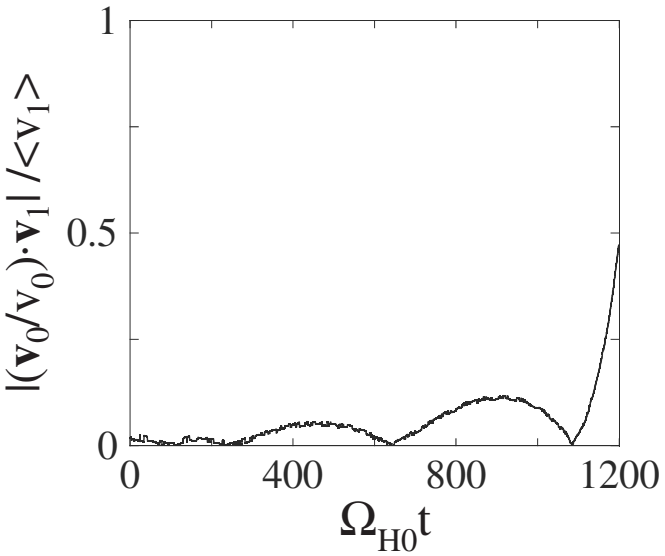

FIG. 6. Time variation of $|(\boldsymbol{v}_0/v_0)\cdot\boldsymbol{v}_1|/\langle v_1\rangle$. The brackets indicate the time averaging over the acceleration time from $\Omega_{H0}t = 0$ to $\Omega_{H0}t = 1200$. The fact that this quantity is much smaller than unity shows that $\boldsymbol{v}_0$ and $\boldsymbol{v}_1$ are nearly perpendicular.

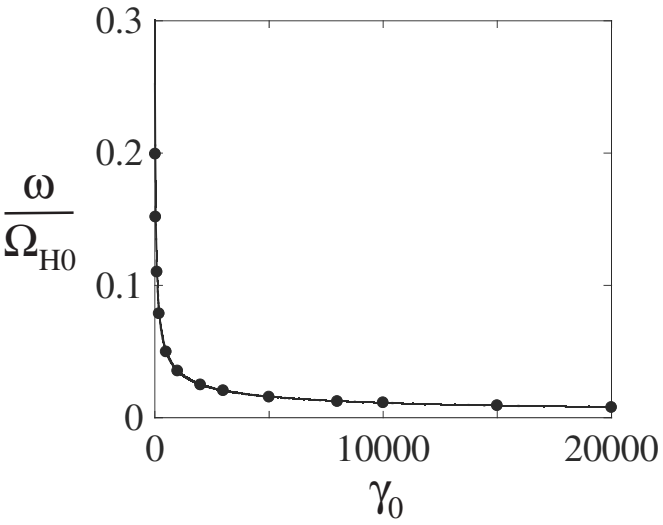

FIG. 7. Perturbation frequency ω vs γ_0. The dots and solid line represent the simulation results and theoretical prediction, respectively. Both of them show that $\omega \sim \gamma_0^{-1/2}$.

particle motion quickly deviates from the zeroth-order solution, it should be attributed to the fact that $f_x' > 0$, since the wave profile is stationary in the test particle calculations. The zeroth-order velocity at this location is $\boldsymbol{v}_0/c \simeq (0.700, -0.119, 0.704)$, which coincides with the initial velocity $\boldsymbol{v}_0$ studied above. We do not find either increase in γ or oscillation of v_x. In the stable case (Fig. 4), the amplitude of the oscillation of v_x at $\Omega_{H0}t=1000$ was less than 0.41% of the initial v_x, while in the present case, v_x decreases by 6.3% by $\Omega_{H0}t=20$. This indicates that the particle quickly goes away from the initial position ξ_0. The magnitude of the perturbed velocity v_{x1} increases with time as $\exp[0.284(\Omega_{H0}t)]$ during the period $2 \leq \Omega_{H0}t \leq 18$. This observed growth rate $\omega/\Omega_{H0}=0.284$ is close to the theoretical value estimated from Eq. (26), $\omega/\Omega_{H0} \simeq 0.260$.

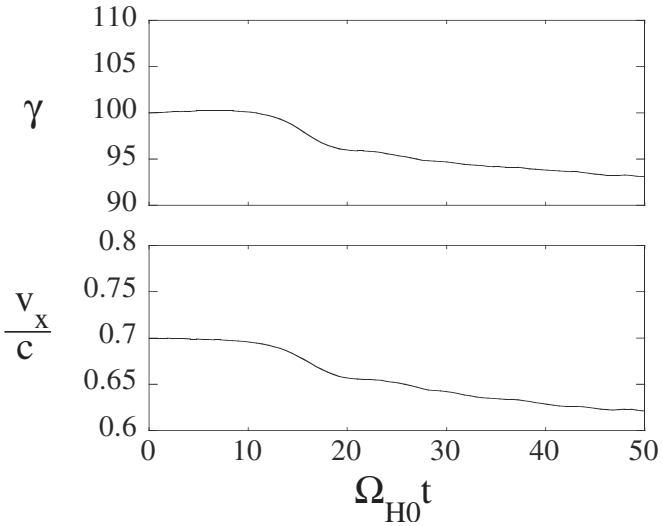

FIG. 8. Time variations of γ and v_x of an unstable ion. This ion is initially put at the position with $f_x' > 0$ and quickly goes away from the initial position. Thus, it does not exhibit energy increase or v_x oscillation.

IV. SUMMARY

With use of computer simulations, we have studied the motion of relativistic ions accelerated in the direction parallel to the magnetic field in a magnetosonic shock wave.

We have briefly described this theory for particles accelerated along the magnetic field; the assumptions, zeroth-order velocity $\boldsymbol{v}_0$ of an accelerated particle, and its energy increase rate. Furthermore, we have discussed its perturbed motion; the perturbation $\boldsymbol{v}_1$ is a one-dimensional oscillation in a plane nearly perpendicular to $\boldsymbol{v}_0$, the frequency of which is proportional to $\gamma^{-1/2}$. From the discussion of the oscillation frequency, the condition for the stability of the perturbed motion is also given.

We have then tested the theory using both particle simulations and test particle calculations; we obtain the fields of a shock wave from a one-dimensional, fully kinetic, electromagnetic simulation, and using these fields we follow test particle orbits. With this method, we have examined the zeroth-order motion, energy increase rate, and perturbation motion (first-order motion) and confirmed that the theoretical predictions and simulation results are consistent.

The zeroth-order theory predicting the acceleration along the magnetic field is applicable to both ions and positrons. The perturbation motions of the ions, however, differ from those of the positrons; the ion perturbation is a one-dimensional oscillation and can be unstable, while the positron perturbation is a stable elliptic oscillation. This difference suggests that, although persistent positron acceleration has been demonstrated with particle simulations (the acceleration continues even if the shock profile varies with time),[18] the ion acceleration in this mechanism can be more fragile.

ACKNOWLEDGMENTS

This work was carried out by the collaboration program, NIFS09KTAN006 of the National Institute for Fusion Science and was supported in part by the Grant-in-Aid for the Scientific Research (C) (Grant No. 20540481) from the Japan Society for the Promotion of Science.

[1] D. Biskamp and H. Welter, Nucl. Fusion **12**, 663 (1972).
[2] D. W. Forslund, K. B. Quest, J. U. Brackbill, and K. Lee, J. Geophys. Res., [Oceans] **89**, 2142, doi:10.1029/JA089iA04p02142 (1984).
[3] Y. Ohsawa, Phys. Fluids **28**, 2130 (1985).
[4] Y. Ohsawa, J. Phys. Soc. Jpn. **59**, 2782 (1990).
[5] B. Lembege and J. M. Dawson, Phys. Fluids B **1**, 1001 (1989).
[6] R. L. Tokar, S. P. Gary, and K. B. Quest, Phys. Fluids **30**, 2569 (1987).
[7] R. Z. Sagdeev and V. D. Shapiro, Zh. Eksp. Teor. Fiz. Pis'ma Red. **17**, 387 (1973) [JETP Lett. **17**, 279 (1973)].
[8] M. A. Lee, V. D. Shapiro, and R. Z. Sagdeev, J. Geophys. Res., [Oceans] **101**, 4777, doi:10.1029/95JA03570 (1996).
[9] V. D. Shapiro and D. Üçer, Planet. Space Sci. **51**, 665 (2003).
[10] M. Toida and Y. Ohsawa, Sol. Phys. **171**, 161 (1997).
[11] N. Bessho and Y. Ohsawa, Phys. Plasmas **6**, 3076 (1999); **9**, 979 (2002).
[12] M. Hoshino and N. Shimada, Astrophys. J. **572**, 880 (2002).
[13] M. Ashour-Abdalla, J. N. Leboeuf, T. Tajima, J. M. Dawson, and C. F. Kennel, Phys. Rev. A **23**, 1906 (1981).
[14] T. P. Armstrong, G. Chen, E. T. Sarris, and S. M. Krimigis, in *Study of Traveling Interplanetary Phenomena*, edited by M. A. Shea and D. F. Smart (Reidel, Dordrecht, 1977), p. 367.
[15] R. B. Decker, Space Sci. Rev. **48**, 195 (1988).
[16] T. Masaki, H. Hasegawa, and Y. Ohsawa, Phys. Plasmas **7**, 529 (2000).
[17] S. Usami and Y. Ohsawa, Phys. Plasmas **9**, 1069 (2002).

[18]H. Hasegawa, S. Usami, and Y. Ohsawa, Phys. Plasmas **10**, 3455 (2003).
[19]H. Hasegawa, K. Kato, and Y. Ohsawa, Phys. Plasmas **12**, 082306 (2005).
[20]S. Usami and Y. Ohsawa, Phys. Plasmas **11**, 3203 (2004).
[21]J. P. Meyer, Astrophys. J., Suppl. **57**, 151 (1985).
[22]S. Takahashi and Y. Ohsawa, Phys. Plasmas **14**, 112305 (2007).
[23]P. A. Sturrock, Astrophys. J. **164**, 529 (1971).
[24]C. F. Kennel and F. V. Coroniti, Astrophys. J. **283**, 694 (1984).
[25]W. H. Press, S. A. Teukolsky, W. T. Vetterling, and B. P. Flannery, *Numerical Recipes in Fortran 77* (Cambridge University Press, New York, 1992).
[26]T. R. McCalla, *Introduction to Numerical Methods and FORTRAN Programming* (Wiley, New York, 1998).
[27]T. Kawashima, S. Miyahara, and Y. Ohsawa, J. Phys. Soc. Jpn. **72**, 1664 (2003).